Level Structure in ^{15}O from the Proton Bombardment of ^{14}N†

M. L. West,* C. M. Jones, J. K. Bair, and H. B. Willard‡

Oak Ridge National Laboratory, Oak Ridge, Tennessee 37830

(Received 5 September 1968)

Absolute cross sections for elastic scattering, ^{14}N$(p, p)^{14}$N, and inelastic scattering, ^{14}N$(p, p_1)^{14}$N*, from the first excited state were measured for proton bombarding energies between 3.7 and 5.67 MeV at laboratory angles of 67.5°, 85.9°, 105.8°, 123.7°, 135.0°, and 157.5° in order to determine level parameters of excited states in ^{15}O. Complete angular distributions were measured at selected energies in this region and limited angular distributions were obtained for inelastic scattering, ^{14}N$(p, p_2)^{14}$N*, from the second excited state, and for the ^{14}N$(p, \alpha)^{11}$C reaction. Scattering anomalies were observed at proton bombarding energies of 3.88, 3.90, 3.99, 4.13, 4.20, 4.575, 4.58, 4.63, 4.74, 4.78, 4.86, 5.02, 5.18, and 5.55 MeV, corresponding to excited states in ^{15}O at 10.91, 10.93, 11.01, 11.14, 11.21, 11.56, 11.565, 11.61, 11.71, 11.75, 11.83, 11.97, 12.12, and 12.47 MeV. Resonances were analyzed using a multilevel R-matrix approximation. Qualitative and semiquantitative fits were made to these data and resonance parameters were determined for many of the observed levels.

INTRODUCTION

THE nucleus ^{15}O consists of eight protons and seven neutrons and, in the shell-model picture, its lowest-order configuration needs only a single nucleon to complete the $(1s)^4(1p)^{12}$ closed shell of ^{16}O. The lower-lying experimental levels (below about 9-MeV excitation energy) of the mirror nuclei ^{15}O and ^{15}N have been compared quite successfully.[1,2] Halbert and French[3] have made theoretical calculations for the even-parity levels of mass-15 nuclei for excitation energies below 15 MeV and these levels have been identified reasonably well with the experimental levels up to about 9 MeV. Theoretical investigations of these nuclei have been hampered by a lack of knowledge of the effective interactions in the more complex shell-model configurations appearing at higher energies and by the absence of precise experimental data on the energy levels appearing above 9-MeV excitation energy.

In the present experiment, absolute differential cross sections have been measured for the elastic and inelastic scattering of protons from ^{14}N for bombarding energies between 3.7 and 5.67 MeV. These data have been analyzed using the R-matrix theory and it has been possible to make semiquantitative fits to the data and to deduce resonance parameters for many of the observed levels in the compound nucleus ^{15}O between 10.9- and 12.5-MeV excitation.

Previous knowledge on the level structure of ^{15}O for proton bombarding energies below 6 MeV has come predominantly from studies of the radiative capture and elastic scattering processes. Duncan and Perry[4]

first studied the ^{14}N$(p, \gamma)^{15}$O reaction by measuring the ground-state decay of ^{15}O for proton bombarding energies between 0.25 and 2.6 MeV (7.52- and 9.72-MeV excitation energy). All presently known energy levels in this region of excitation were observed. The elastic scattering of protons by ^{14}N has been studied by numerous authors[5-16] for bombarding energies below 4.0 MeV (11.02-MeV excitation). Olness, Verona, and Lewis[10] also measured inelastic cross sections for two levels near 3.9 and 3.98 MeV (10.93- and 11.00-MeV excitation). Above 4.0-MeV bombarding energy, there are no published experimental data on the elastic scattering of protons by ^{14}N. However, Kuan et al.[17] at Stanford have recently reported on measurements made in this energy region. Bair et al.[18] studied the ^{14}N$(p, p'\gamma)^{14}$N reaction for bombarding energies between 2.5 and 5.1 MeV and observed two new levels near 4.8 and 4.89 MeV (11.77- and 11.85-MeV excitation), but no spin and parity assignments could be made from their work.

The resonance energies and widths of most of the levels below 4.0 MeV have been determined with fair

[1] E. K. Warburton, J. W. Olness, and D. E. Alburger, Phys. Rev. 140, 1202 (1965).

[2] A. E. Evans, B. Brown, and J. B. Marion, Phys. Rev. 149, 863 (1966).

[3] E. C. Halbert and J. B. French, Phys. Rev. 105, 1563 (1957).

[4] D. B. Duncan and J. E. Perry, Phys. Rev. 82, 809 (1951).

[5] T. S. Webb, C. W. Li, and W. A. Fowler, Phys. Rev. 92, 1084 (1953).

[6] H. E. Gove, A. J. Ferguson, and J. T. Sample, Phys. Rev. 93, 928 (1954).

[7] G. W. Tautfest and S. Rubin, Phys. Rev. 103, 196 (1956).

[8] C. R. Bolmgren, G. D. Freier, J. G. Likeley, and F. K. Famularo, Phys. Rev. 105, 210 (1957).

[9] F. B. Hagedorn, F. S. Mozer, T. S. Webb, W. A. Fowler, and C. C. Lauritsen, Phys. Rev. 105, 219 (1957).

[10] J. W. Olness, J. Verona, and H. W. Lewis, Phys. Rev. 112, 475 (1958).

[11] A. J. Ferguson, R. L. Clarke, H. E. Gove, and J. T. Sample, Chalk River Laboratory Report No. PD-26, 1956 (unpublished).

[12] A. J. Ferguson, R. L. Clarke, and H. E. Gove, Phys. Rev. 115, 1655 (1959).

[13] A. J. Ferguson, Phys. Rev. 115, 1660 (1959).

[14] S. Bashkin, R. R. Carlson, and R. A. Douglas, Phys. Rev. 114, 1552 (1959).

[15] A. K. Val'ter, A. S. Deineko, I. Ya. Malakhov, P. V. Sorokin, and A. Ya. Taramov, Izzv. Akad. Nauk SSSR 23, 228 (1959).

[16] J. Cohen-Ganouna, M. Lambert, and J. Schmouker, J. Phys. (Paris) 24, 43 (1963).

[17] H. M. Kuan, S. S. Hanna, and M. Hasinoff, Bull. Am. Phys. Soc. 12, 52 (1967).

[18] J. K. Bair, H. O. Cohn, J. D. Kington, and H. B. Willard, Phys. Rev. 104, 1595 (1956).

accuracy, but unambiguous spin and parity assignments have been obtained for only a few of the levels. Difficulty of analysis has been attributed to the anomalously large background of potential scattering and the complications inherent in the interaction of nonzero spin particles.

EXPERIMENTAL PROCEDURE

A differentially pumped gaseous target scattering chamber containing 99.98% pure natural nitrogen gas was used for the cross-section measurements.[19] The chamber consists of a cylindrical shell equipped with a removable cover and a movable lower section attached through a rotating vacuum seal. A movable counter, mounted in the lower section, could view scattered particles at all angles between 20° and 160° with respect to the incident beam. Portholes positioned at intervals around the chamber housing allowed fixed detectors to be placed at any of 11 angles. The effective target volume for scattered particles was determined by precision slit systems associated with each detector.

Protons from the Oak Ridge National Laboratory 5.5-MV Van de Graaff accelerator were analyzed by a 90° magnet. The incident beam energy was determined by calibrating the analyzing magnet with the known resonance at 4.808 ± 0.008 MeV in the $^{12}C(p, p)^{12}C$ reaction.[20] The direct proton beam was collected in a Faraday cup at the rear of the chamber and the total current was determined by conventional beam integration techniques.

Scattered particles were detected by surface barrier detectors placed at selected angles in the chamber. Pulses from these detectors were fed through linear amplifiers and into a multiplex routing and mixing circuit[21] for storage in a multichannel analyzer. The multiplex unit served to divide the analyzer into the equivalent of three separate 512-channel analyzers with the pulses from each detector stored separately.

The procedure for each run included the recording of target pressure, chamber temperature, integrated beam current, beam energy, and total particle yield for each counter. The energy spectrum of pulses from each counter was permanently recorded on magnetic tape for future analysis. Two complete sweeps were made over the energy range 3.71–5.67 MeV, and three counters were operated simultaneously to give a total of six excitation functions. Energy steps varied between 3 and 5 keV, depending on the behavior of the cross section. A series of complete angular distributions was also taken with the moving counter at selected energies in this energy range.

The pulse-height spectra were analyzed with a com-

puter program[22] which, after background subtraction, fits a peak in the spectrum with a modified normal distribution. Appropriate corrections were made to these data for heating of the nitrogen gas by the beam and for rate-dependent losses in the scalers. These corrections were typically about 1%. Typical dead-timec orrections ranged from 5 to 20%. A number of small corrections not made to these data included slit edge scattering, detector efficiency, and the loss of beam between target volume and Faraday cup. Subsequent work[23] on the scattering chamber indicated that these effects were less than a few tenths percent. In addition to these ignored effects, it was later discovered that the magnetic secondary electron suppressor system of the Faraday cup was not completely effective. The Faraday cup used in this work was subsequently replaced with the Faraday cup described in Ref. 19.

Experimental uncertainties in the cross-section measurements resulted in an estimated normal distribution uncertainty with a standard deviation of $\pm4\%$ exclusive of counting statistics. Statistical uncertainties varied between 0.2 and 0.5% for all elastic cross sections and between 2 and 3% for all inelastic cross sections.

Uncertainties in the bombarding energy resulted from uncertainties in the calculated energy loss of protons passing through the nitrogen gas, uncertainties in the magnetic calibration constant, finite beam resolution, finite target thickness, and straggling of the beam in the chamber gas. Energy losses of protons passing through the chamber gas were determined by observing energy shifts of the $^{12}C(p, p)^{12}C$ resonance as a function of chamber pressure. The uncertainty in this determination was about 3.3 keV for typical operating conditions. Straggling of the beam for a typical energy and pressure (5.0 MeV and 9 mm Hg) resulted in an asymmetric distribution $(\lambda=1.25)$[24] with a standard deviation of ±3 keV. Typical target thickness was about 0.5 keV. Accuracy of the absolute energy scale was estimated to be ±15 keV. The relative accuracy is better although in some cases it was necessary to shift excitation functions measured at different times by as much as 5 keV to produce a satisfactory match.

EXPERIMENTAL RESULTS

Absolute differential cross sections for elastic scattering, $^{14}N(p, p)^{14}N$, and inelastic scattering, $^{14}N(p, p_1)^{14}N^*$, from the first excited state of $^{14}N(Q=-2.311$ MeV) were measured at laboratory angles of 67.5°, 85.9°, 105.8°, 123.7°, 135.0°, and 157.5° for the proton bombarding energy range 3.7–5.67 MeV (Figs. 1–4). In addition, complete angular distributions (Figs. 5 and 6) were measured at selected energies in this region and limited angular distributions (Figs. 7 and 8) were

[19] C. M. Jones, J. W. Johnson, and R. M. Beckers, Nucl. Instr. Methods (to be published).
[20] C. W. Reich, G. C. Phillips, and J. L. Russell, Jr., Phys. Rev. 104, 143 (1956).
[21] Designed at Oak Ridge National Laboratory.

[22] We are indebted to J. K. Dickens (ORNL) for the use of this program.
[23] M. D. Mancusi, J. K. Bair, C. M. Jones, S. T. Thornton, and H. B. Willard, Nucl. Instr. Methods (to be published).
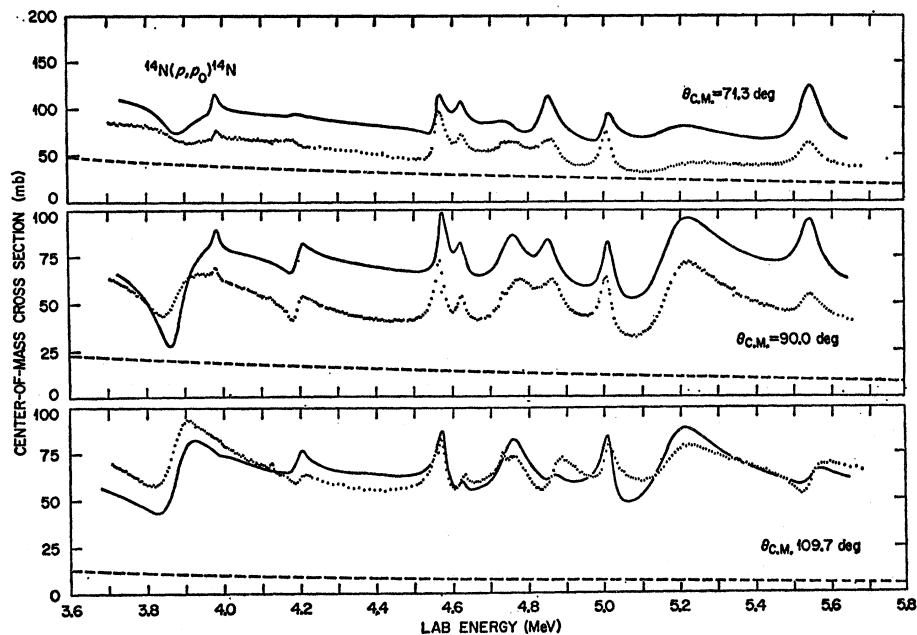[24] B. B. Rossi, High-Energy Particles (Prentice-Hall, Inc., Englewood Cliffs, N.J., 1952).

FIG. 1. Differential cross sections for the elastic scattering of protons from ^{14}N as a function of incident proton energy at scattering angles of 71.3°, 90.0°, and 109.7°. Solid curves are theoretical fits and dashed curves are the Rutherford cross section.

obtained for inelastic scattering, ^{14}N$(p, p_2)^{14}$N*, from the second excited state of ^{14}N$(Q=-3.95$ MeV) and for the ^{14}N$(p, \alpha)^{11}$C reaction. All cross sections except the inelastic excitation functions are in the c.m. system and all energies are laboratory bombarding energies at the center of the target. In Figs. 5 and 6, cross sections taken from the complete angular distribution measurements (closed points) and those from the excitation function measurements (open points) are plotted together and indicate the reproducibility of these

data. The statistical uncertainty is indicated for each datum point.

ANALYSIS

An inspection of Figs. 1–4 shows that many resonances were observed in the experimental elastic-scattering cross section and that several of these resonances has significant partial widths for the inelastic channel. Analysis of these data was carried out using the Wigner R-matrix formalism as presented by Lane and Thomas.[25]
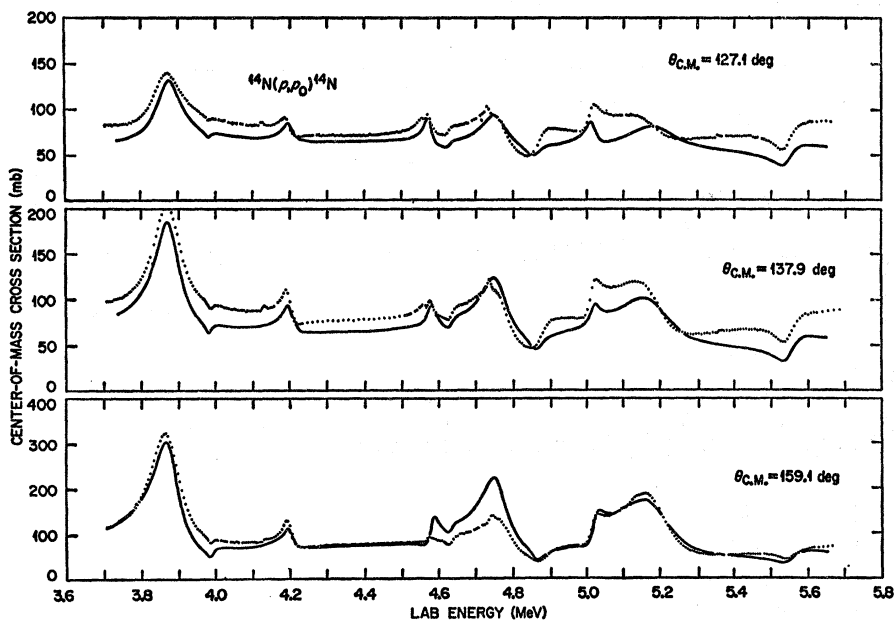

FIG. 2. Differential cross sections for the elastic scattering of protons from ^{14}N as a function of incident proton energy at scattering angles of 127.1°, 137.9°, and 159.1°. Solid curves are theoretical fits. The Rutherford cross section is well below 16 mb at all angles shown.

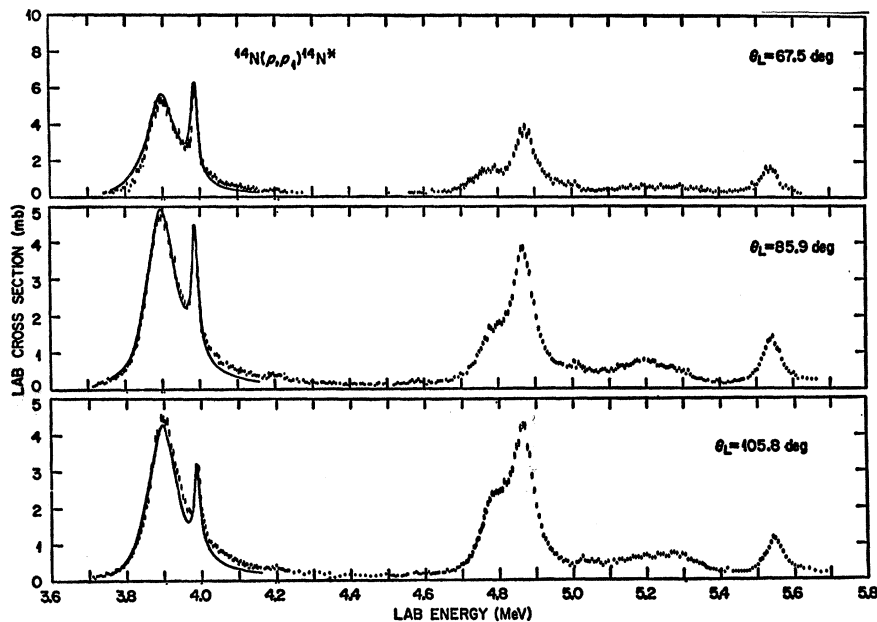[25] A. M. Lane and R. G. Thomas, Rev. Mod. Phys. **30**, 257 (1958).

FIG. 3. Differential cross sections for protons from the ^{14}N (p, p_1) ^{14}N* reaction $(Q= -2.31$ MeV$)$ as a function of incident proton energy at laboratory scattering angles of 67.5°, 85.9°, and 105.2°. Solid curves are theoretical fits.

First, off-resonance elastic angular distributions were analyzed to determine the behavior of slowly varying nonresonant phases. The elastic excitation functions were then studied to determine the interference of nuclear scattering amplitudes with the Coulomb and slowly varying background amplitudes (determined from off-resonance analysis). Since the qualitative shape and magnitude of this interference depends strongly upon the assumed value of l and J, the total angular momentum and parity of a resonance may be obtained from this analysis. A study of inelastic angular distributions gave an independent determination of

resonance spin and parity, and permitted a detailed analysis of interference between interfering levels, and yielded values for inelastic widths. The inelastic excitation functions were used to determine resonance energies and total widths.

^{14}N(p, p)^{14}N Elastic Scattering

Since many of the levels under investigations were broad and overlapping, it was necessary to consider many states of different spins and parities simultaneously. Two-level scattering formulas were used so interference between levels of the same spin and parity

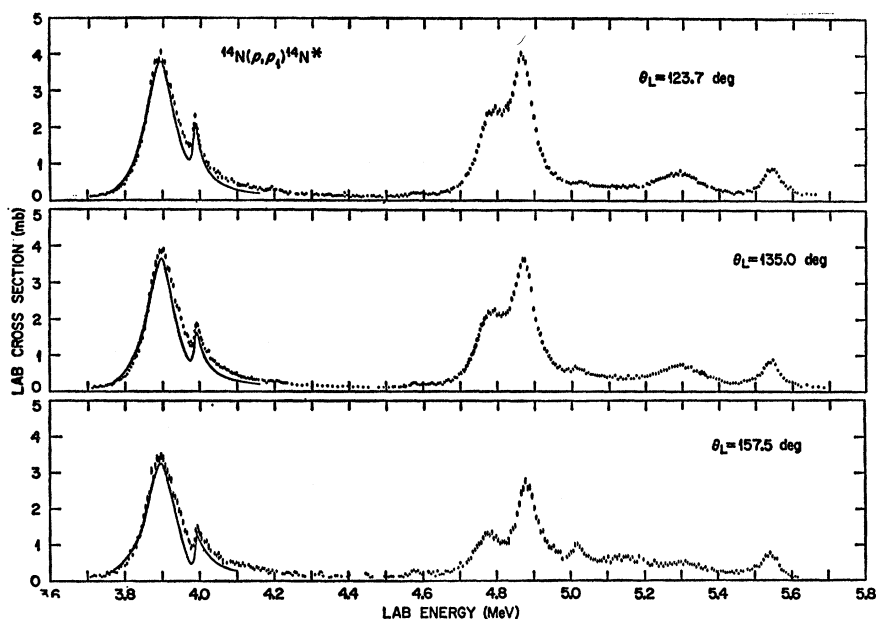FIG. 4. Differential cross sections for protons from the ^{14}N (p, p_1) ^{14}N* reaction $(Q= -2.31$ MeV$)$ as a function of incident proton energy at laboratory scattering angles of 123.7°, 135.0°, and 157.5°. Solid curves are theoretical fits.
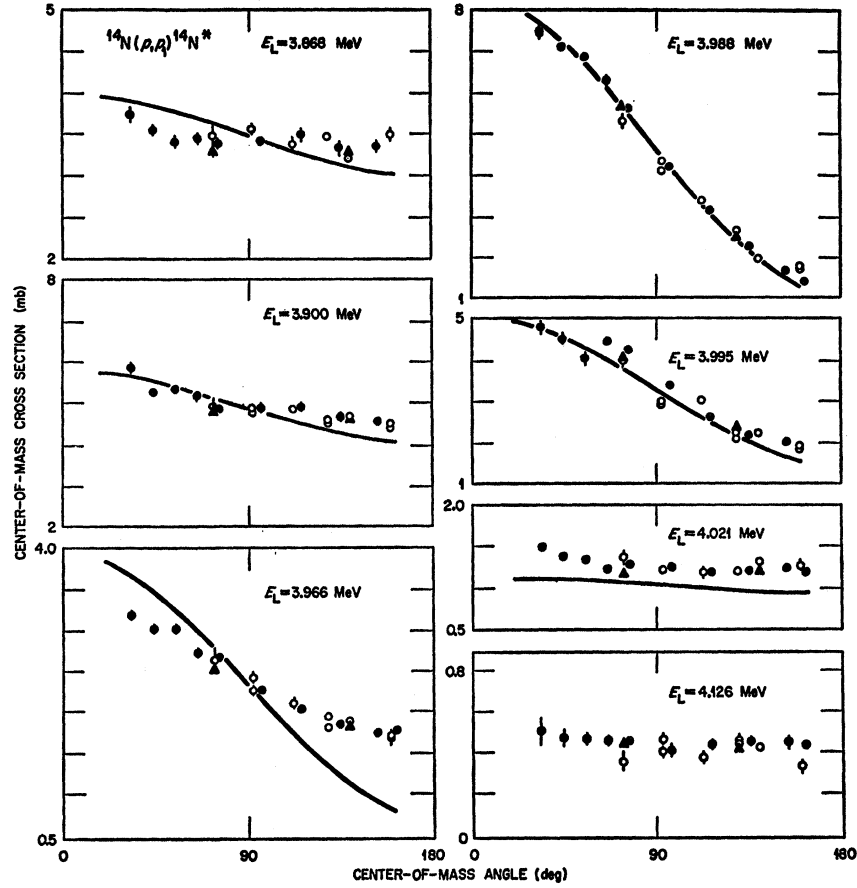
FIG. 5. Angular distributions of protons from the ^{14}N$(p, p_1)^{14}$N reaction $(Q=-2.31$ MeV). The solid curves are theoretical fits for the s-wave formation of a 90-keV wide $J=\frac{1}{2}^+$ state at 3.90 MeV interfering with the p-wave formation of a 20-keV wide $J=\frac{1}{2}^-$ state at 3.988 MeV.

in close proximity could be treated exactly. The theoretical differential cross section is given as a sum over scattering amplitudes $A_{s'm_{s'},sm_s}$, with each amplitude designating one of the possible channel spin configurations $(sm_s \rightarrow s'm_{s'})$,

$$d\sigma_{\alpha,\alpha'}(\theta, \varphi) = [(2I_1+1)(2I_2+1)]^{-1}$$

$$\times \sum_{ss',m_s m_{s'}} | A_{\alpha's'm_{s'},\alpha sm_s} |^2 d\Omega_{\alpha'}, \quad (1)$$

where

$$A_{\alpha's'm_{s'},\alpha sm_s} = -(\sqrt{\pi}/k)\{[C(\theta)+p(\theta)]\delta_{\alpha's'm_{s'},\alpha sm_s}$$

$$+i\sum_{JMll'm_{l'}} (2l+1)^{1/2}(slm_s 0 \mid JM)(s'l'm_{s'}m_{l'} \mid JM)$$

$$\times X^J_{\alpha's'l',\alpha sl} Y_{l'm_{l'}}(\Omega_{\alpha'})\}. \quad (2)$$

Here α gives the type of incoming particle and the state of the struck nucleus, s is the channel spin obtained from vector addition of the intrinsic spins of the incoming particle and target nucleus $(I_1$ and I_2, respectively), and m_s is the channel-spin projection. The sum over J represents the sum over all resonances that are treated explicitly, and l is the orbital angular momentum; M and m_l are the total and orbital angular momentum projections, respectively. The primes refer

to quantities in the outgoing channels (for elastic scattering $\alpha = \alpha'$).

In the scattering amplitude of Eq. (2), k is the wave number of relative motion,

$$k = (2\mu E/\hbar^2)^{1/2}, \quad (3)$$

where E is the energy of relative motion of the pair of incoming particles and μ is their reduced mass. $C(\theta)$ is the Rutherford amplitude of Coulomb scattering for angle θ:

$$C(\theta) = (4\pi)^{-1/2}\eta \, \mathrm{cosec}^2\tfrac{1}{2}\theta \, \exp[-2i\eta \, \ln(\sin\tfrac{1}{2}\theta)],$$

with

$$\eta \equiv Z_1 Z_2 e^2 \mu/\hbar k. \quad (4)$$

$p(\theta)$ is the potential scattering amplitude,

$$p(\theta) = \pi^{-1/2}\sum_l (2l+1) \, \sin\varphi_l \, \exp[i(2\omega_l - \delta_{sl})]P_l(\cos\theta),$$

$$(5)$$

where the δ_{sl} are potential phase shifts for off-resonance scattering [not to be confused with the Kronecker δ's in Eq. (2)] and the ω_l are Coulomb phase shifts:

$$\omega_l \equiv \sum_{m=1}^{l} \tan^{-1}\frac{\eta}{m}, \qquad \omega_0 = 0. \quad (6)$$
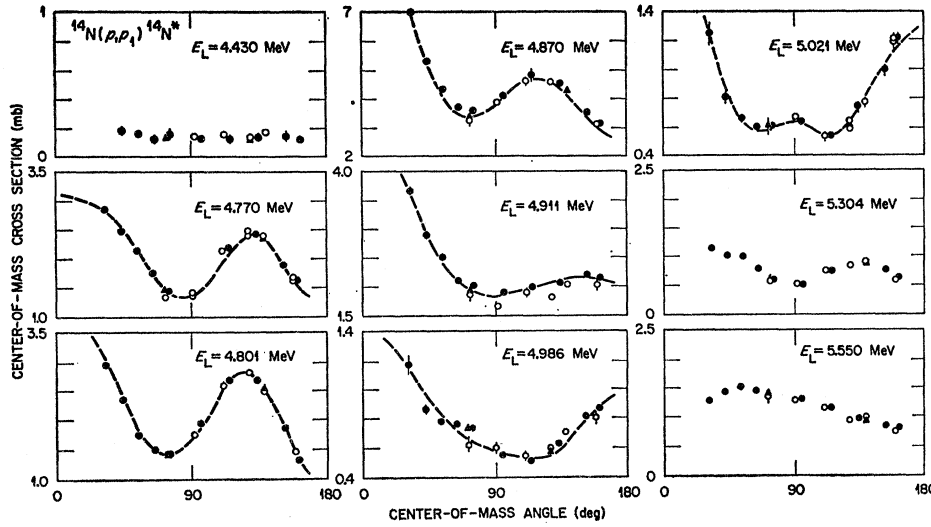
FIG. 6. Angular distributions of protons from the $^{14}N(p, p_1)^{14}N^*$ reaction ($Q=-2.31$ MeV). The dashed lines are least-squares Legendre-polynomial fits to the data.

The symbols $(slm_s0 \mid JM)$ and $(s'l'm_{s'}m_{l'} \mid JM)$ are the usual Clebsch-Gordan coefficients.

The generally nondiagonal matrix X^J describes resonance scattering and in the two-level approximation has elements

$$X^J_{s'l',sl} = 2 \exp[i(\omega_l + \omega_{l'} - \delta_l - \delta_{l'})](\mathcal{P}_l \mathcal{P}_{l'})^{1/2}$$

$$\times \sum_{\lambda\mu=1,2} \gamma_{\lambda ls}\gamma_{\mu l's'}A_{\lambda\mu}{}^J, \quad (7)$$

$$A_{11}{}^J = (E_2{}^J - E - \xi_{22}{}^J)/D^J,$$

$$A_{22}{}^J = (E_1{}^J - E - \xi_{11}{}^J)/D^J,$$

$$A_{12}{}^J = A_{21}{}^J = \xi_{12}{}^J/D^J,$$

$$D^J = A_{11}{}^J A_{22}{}^J - (A_{12}{}^J)^2.$$

The elements of $\xi_{\lambda\mu}{}^J$ are separated into real and imaginary parts:

$$\xi_{\lambda\mu}{}^J = -\Delta_{\lambda\mu}{}^J + \tfrac{1}{2}i\Gamma_{\lambda\mu}{}^J, \quad \lambda, \mu = 1, 2 \quad (8)$$

where the $\Delta_{\lambda\mu}{}^J$ are elements of the shift matrix,

$$\Delta_{\lambda\mu}{}^J = \sum_{\alpha sl} \gamma_{\lambda sl}{}^J \gamma_{\mu sl}{}^J (S_l - B_l{}^J), \quad (9)$$

and the $\Gamma_{\lambda\mu}$ are elements of the width matrix,

$$\Gamma_{\lambda\mu}{}^J = \sum_{\alpha sl} \mathcal{P}_l \gamma_{\lambda sl}{}^J \gamma_{\mu sl}{}^J. \quad (10)$$

In these equations λ, μ represents the sum over two levels of the same spin and parity; $E_1{}^J$ and $E_2{}^J$ are the energies of the two levels and E is the c.m. bombarding
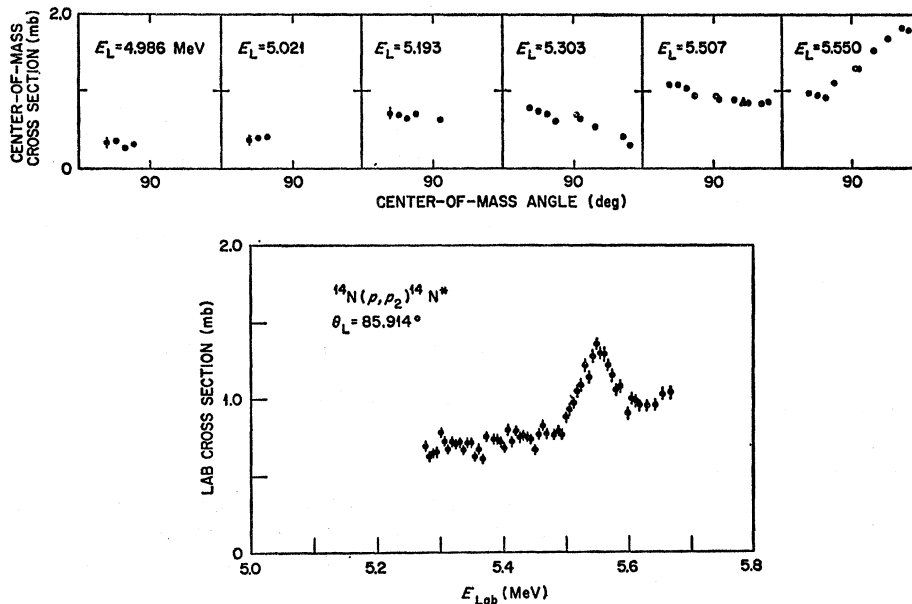

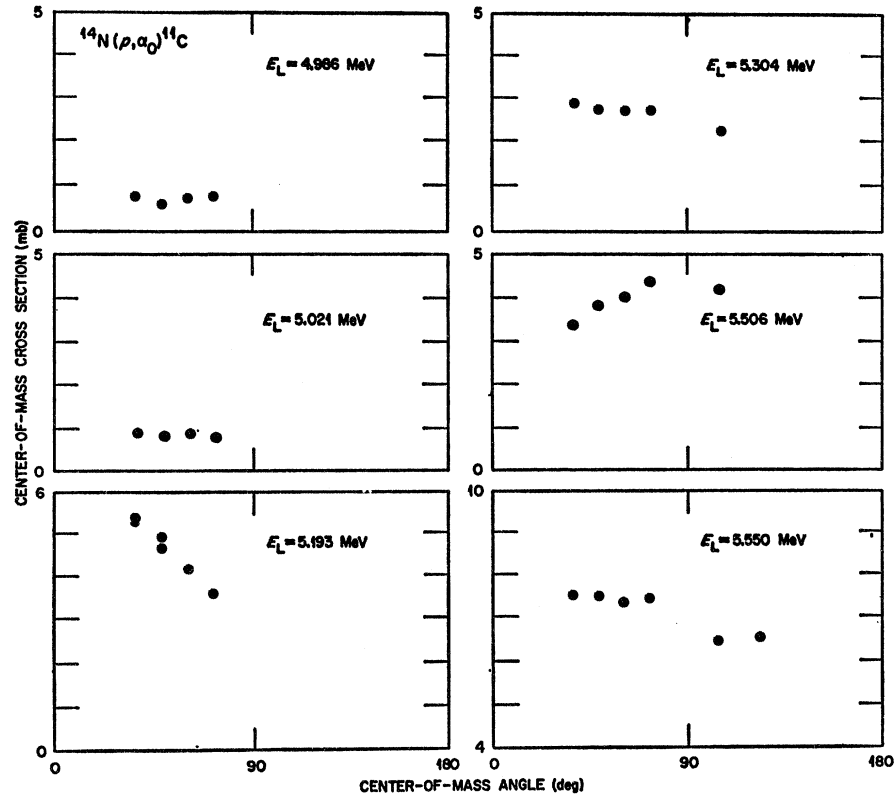FIG. 7. Differential cross sections for protons from the $^{14}N(p, p_2)^{14}N^*$ reaction ($Q=-3.95$ MeV).

FIG. 8. Differential cross sections for protons from the ¹⁴N(p, α)¹¹C reaction.

energy; $\mathcal{P}_l$ is the penetrability,

$$\mathcal{P}_l = ka/(F_l^2 + G_l^2), \tag{11}$$

where F_l and G_l are the regular and irregular Coulomb wave functions evaluated at the nuclear radius a. S_l is the energy shift,

$$S_l = ka(F_l F_{l'} + G_l G_{l'})/(F_l^2 + G_l^2). \tag{12}$$

B_l is the arbitrary boundary-value parameter and $\gamma_{\lambda sl}{}^J$ is the reduced width amplitude of the λth level of spin J formed through the channel (sl). The reduced width amplitudes $\gamma_{\lambda sl}{}^J$ are expressed in terms of a channel-spin ratio $\alpha_{\lambda sl}{}^J$ by

$$\gamma_{\lambda sl}{}^J = \alpha_{\lambda sl}{}^J \gamma_{\lambda l}{}^J, \tag{13}$$

with the coefficients normalized to unity:

$$\sum_s (\alpha_{\lambda sl}{}^J)^2 = 1. \tag{14}$$

The $\alpha_{\lambda sl}$ give an indication of the channel-spin dependence of a level formed through a particular partial wave l.

These theoretical expressions for the differential cross section were programmed for a CDC 1604 computer. This code was made sufficiently general so the elastic scattering of charged or uncharged particles of arbitrary spin could be analyzed. As many as 16 resonance pairs, each pair designating resonances of the same spin and

parity, can be treated simultaneously. Input to the code is in the form of trial resonance parameters and various forms are allowed for the potential phase shifts δ_l. Output is in the form of computer-plotted excitation functions. Both experimental and theoretical cross sections may be plotted as an aid to the analysis.

For the case of protons of spins $\frac{1}{2}$ incident upon ¹⁴N of spin 1, the possible channel spins are $\frac{1}{2}$ and $\frac{3}{2}$; hence there are six channel-spin projections m_s and up to 36 scattering amplitudes $A_{s'm_s',sm_s}$ to be determined. Each level can be formed by two partial waves and the value of l can change during the scattering process. The initial method of analysis was to study theoretical resonance shapes for various assignments of l, J, π, and channel spin. However, before this could be done it was necessary to have an adequate description of the background scattering.

Background processes are described by scattering amplitudes

$$A_{\alpha's'm_s',\alpha sm_s} = -(\pi^{1/2}/k)[C(\theta) + p(\theta)]\delta_{\alpha's'm_s',\alpha sm_s}, \tag{15}$$

where $C(\theta)$ and $p(\theta)$ are defined by Eqs. (4) and (5), respectively. A fit to the off-resonance scattering was attempted by varying the phase shifts δ_{sl} [see Eq. (5)]. For a truly isolated resonance, these phase shifts reduce to the hard-sphere values
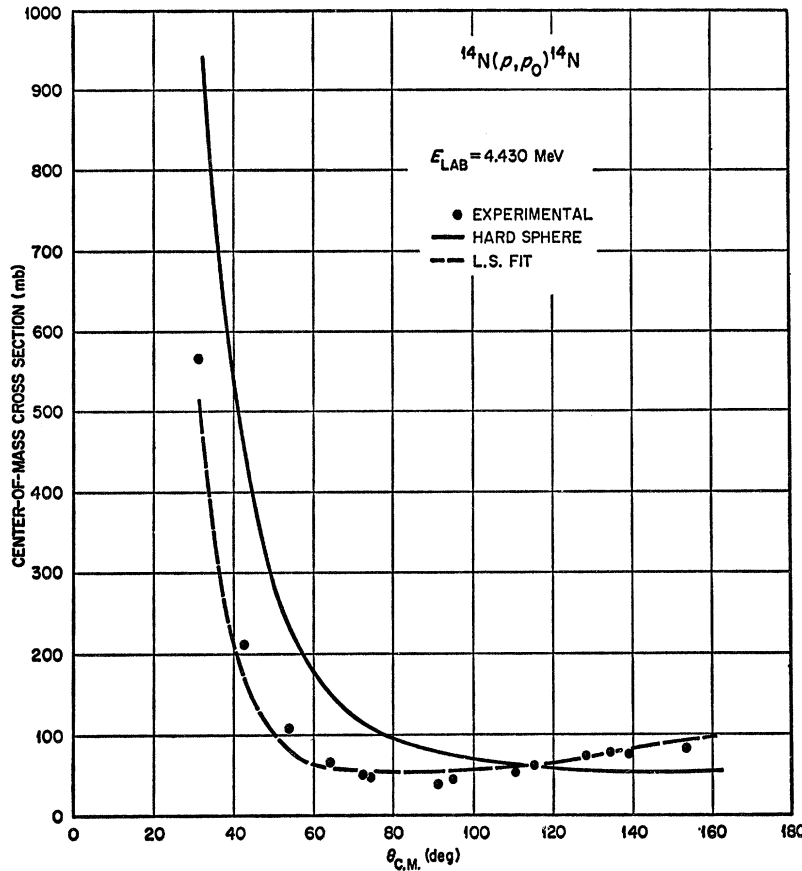
$$\delta_{sl} = \varphi_l = \tan^{-1}(F_l/G_l)_a, \tag{16}$$

FIG. 9. Theoretical fits to the approximately off-resonance angular distribution for the elastic scattering of protons from ^{14}N at 4.43 MeV.

which depend only on l. In practice, it is this l-dependent set of phase shifts that is varied to fit the background. This procedure is justified if the φ_l are not allowed to deviate far from the theoretical values. An anomalously large background is expected to be J-dependent and can best be treated by including arbitrary resonance terms with large total widths.

A least-squares fit was made to the approximate off-resonance angular distribution at 4.43 MeV and this

FIG. 10. Theoretical values of the hard-sphere phase shifts (ϕ_l) as a function of energy for protons elastically scattered from ^{14}N.

set of phase shifts was used as a starting point in determining a set of φ_l that would reasonably approximate background scattering at all energies. Figure 9 shows the least-squares fit and the predicted hard-sphere background. The theoretical hard-sphere phase shifts are shown in Fig. 10 and the set of phases used in this analysis are as follows:

$$\varphi_0 = \Phi_0(\text{hard sphere}) + 10.0°$$

$$\varphi_1 = 12.0°, \quad \varphi_2 = 2.0°, \quad \varphi_3 = 1.0°. \tag{17}$$

These phase shifts represent a reasonable fit to the data and are not necessarily a unique description of the actual scattering. This set of phases did not deviate drastically from the hard-sphere values; in particular, the phase shifts for $l = 0$ (which accounted for a majority of the scattering) was very near Φ_0 (hard sphere). Since qualitative shapes for resonances did not depend strongly on variations in the higher ($l \geq 1$) phase shifts and since there were not enough off-resonance angular distributions to determine their actual energy dependence, the phase shifts for $l \geq 1$ were taken from the least-squares fit at 4.43 MeV.

A least-squares fit was also made to the 4.43-MeV angular distribution by assuming a set of phases that depended on the incident target spin. This led to a set of phase shifts $\delta_{l+1/2}$, $\delta_{l-1/2}$ which described scattering

FIG. 11. Theoretical single-level resonance shapes for the elastic scattering of protons from ^{14}N at $E_0=4.0$ MeV.
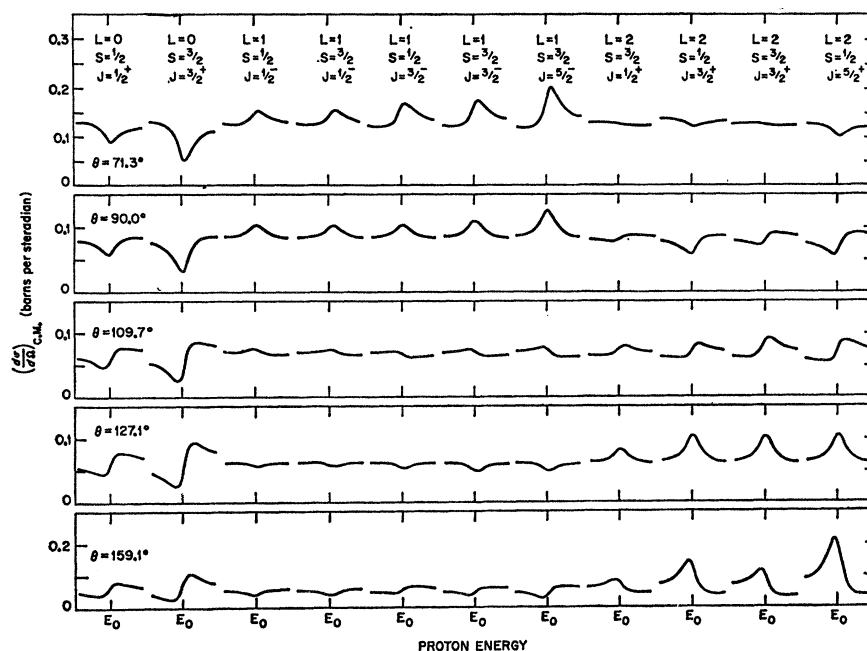
by a potential which depends on coupling of the incident particle spin with the orbital angular momentum. The slight improvement in fit over that for l-dependent phase shifts did not justify the complicated procedure necessary for including these phase shifts in the general analysis. If there had existed a more complete set of off-resonance angular distributions at several energies so that a complete set of phases could have been determined accurately, such an analysis would have been justified.

An optical-model search was also made on the off-resonance scattering but this proved unsuccessful. No realistic set of optical parameters could be found that would produce a satisfactory fit. Insufficient off-resonance data and complications introduced by target spins made this analysis difficult.

Next, theoretical resonance shapes were calculated for each allowed combination of l, s, J, and π. Figures 11 and 12 show these shapes for a resonance energy of 4.0 MeV (indicated by E_0). Partial-wave functions for $l=0$ to 4 are shown with their corresponding channel-spin and total-spin assignments. The angles shown are the c.m. angles. (The theoretical shapes for 137.9° are not shown because they differ only in magnitude from the 127.1° and 154.1° curves). Resonances show distinctive energy-dependent shapes for the various l-wave formations and resonances formed by a particular l wave show a characteristic variation with angle. Resonance shapes were calculated for extreme variations of the background phase shifts and it was noted that the over-all characteristic shape for each partial-wave formation did not change. However, the resonance magnitude and detailed shape were sensitive to assumed values of the background.

These theoretical curves were then compared to the experimentally observed resonances to give an initial guess on resonance parameters. These parameters were then adjusted for a best fit to the data.

^{14}N$(p, p_1)^{14}$N* Inelastic Scattering

Distinct resonance phenomena were observed in this inelastic channel at proton bombarding energies of 3.9, 3.99, 4.78, 4.86, and 5.55 MeV (Figs. 3 and 4). Analysis of the inelastic angular distributions helped to resolve ambiguities remaining after the elastic analysis and played an essential role in the assignment of parameters to these states.

Theoretical expressions for the differential cross section similar to Eqs. (1) and (2) but based on the single-level approximation were programmed for the CDC 1604 computer. For this case, the resonance amplitude $X_{\alpha's'l',\alpha sl}{}^J$ is given by

$$X_{\alpha's'l',\alpha sl}{}^J$$

$$= \frac{\exp[i(\omega_{\alpha l}-\varphi_{\alpha l})]\exp[i(\omega_{\alpha'l'}-\varphi_{\alpha'l'})](\Gamma_{\alpha sl}\Gamma_{\alpha's'l'})^{1/2}}{E_0+\Delta-E-\frac{1}{2}i\Gamma_T{}^J},$$

$$(18)$$

where α and α' denote the elastic incoming and the inelastic outgoing channels, respectively. The partial width $\Gamma_{\alpha sl}$ is given by

$$\Gamma_{\alpha sl}=2\mathcal{P}_l(\gamma_{\alpha sl})^2, \qquad (19)$$

the level shift Δ is

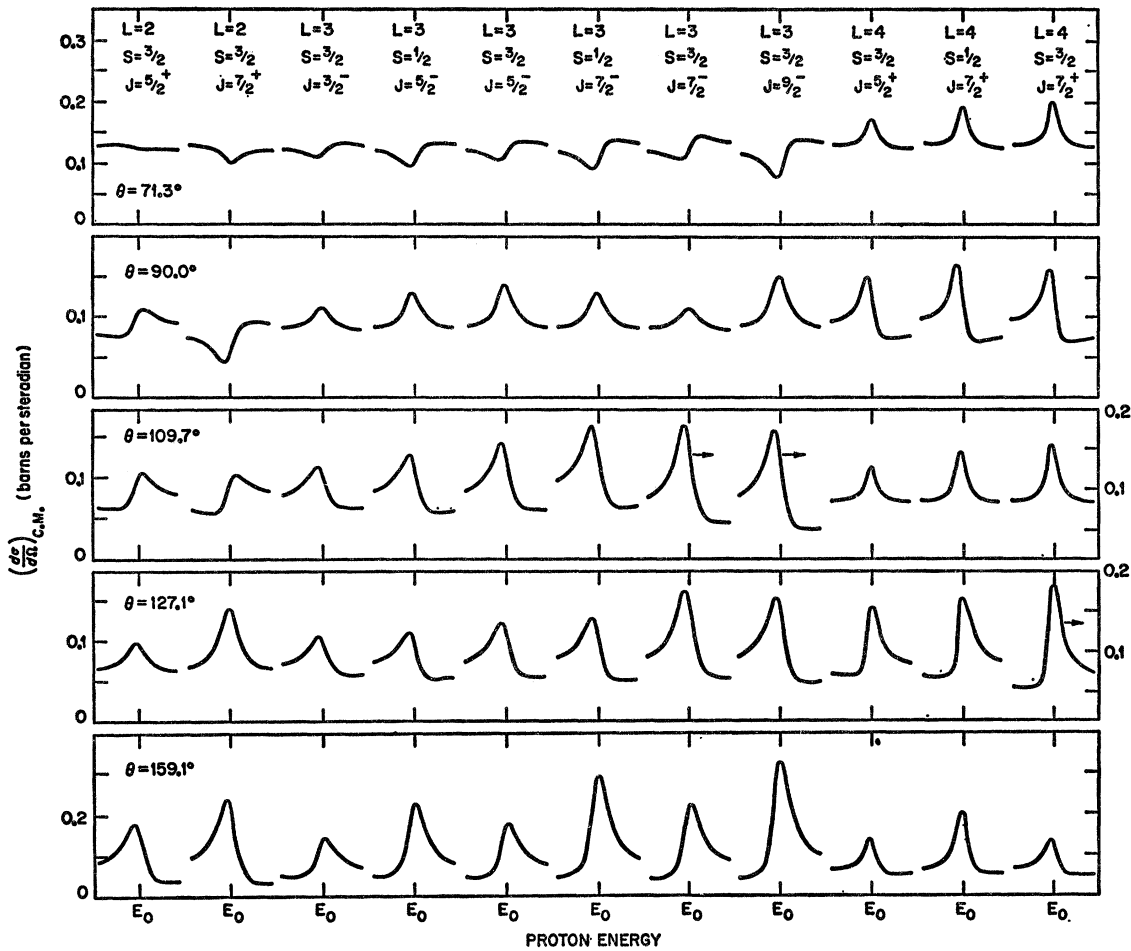$$\Delta=\sum_{\alpha sl}(S_{\alpha sl}-B_{\alpha sl})(\gamma_{\alpha sl})^2, \qquad (20)$$

FIG. 12. Theoretical single-level resonance shapes for the elastic scattering of protons from ^{14}N at $E_0=4.0$ MeV.

and the total width Γ_T is

$$\Gamma_T = \sum_{\alpha s l} \Gamma_{\alpha s l} = \sum_{\alpha} \Gamma_{\alpha}, \qquad (21)$$

where α is summed over the elastic and inelastic channels.

Output of this code is in the form of computer-plotted angular distributions, and as many as five resonances of different spins and parities can be treated simultaneously.

In addition to these calculations, theoretical equations for the angular distributions expressed as a sum of Legendre polynomials were studied and compared to least-squares Legendre polynomial fits to the data. Angular-distribution shapes depend on the total-spin assignments; for a particular assignment they are also quite sensitive to the channel-spin mixture. Hence, a comparison of these theoretical expressions to the least-squares fits restricts total-spin and channel-spin assignments and allows one to obtain qualitative information on level formation and decay. The inelastic analysis is somewhat simplified because states decaying through

this channel are limited to an outgoing channel spin of $\frac{1}{2}$ and a single-partial wave. Of course, both channel spins and two-partial waves are allowed for the incoming channel (see Table I).

TABLE I. Allowed values of the orbital angular momentum l for states in ^{15}O formed by $p+^{14}$N. p_0 and p_1 are the elastic and inelastic channels, respectively. s is the channel spin.

J^π	l_{p_0}		l_{p_1} [a]
	$s=\frac{1}{2}$	$s=\frac{3}{2}$	$s=\frac{1}{2}$
$\frac{1}{2}^+$	0	2	0
$\frac{1}{2}^-$	1	1	1
$\frac{3}{2}^+$	2	0, 2	2
$\frac{3}{2}^-$	1	1, 3	1
$\frac{5}{2}^+$	2	2, 4	2
$\frac{5}{2}^-$	3	1, 3	3
$\frac{7}{2}^+$	4	2, 4	4
$\frac{7}{2}^-$	3	3, 5	3

[a] Channel spin $s=\frac{3}{2}$ is not allowed for the inelastically scattered protons.

TABLE II. Resonance parameters used to fit the $^{14}N(p, p_0)^{14}N$ and $^{14}N(p, p_1)^{14}N$ experimental cross sections shown in Figs. 1–6. E_p is the incident proton energy and E_x is the excitation energy in ^{15}O. J^π is the total-spin and parity assignment (alternative assignments are shown in parentheses). Γ_T, Γ_e, and Γ_i are the total width, elastic width, and inelastic width, respectively ($\Gamma_T = \Gamma_e + \Gamma_i$). l_0 and s_0 are the orbital angular momentum and channel spin for the incident and elastically scattered proton; l_1 is the orbital angular momentum of the inelastically scattered proton. $\gamma_{p_0 l_0 s_0}^2$ and $\gamma_{p_1 l_1}^{1/2^2}$ are reduced widths ($\Gamma_j = 2\mathcal{P}\gamma_j^2$) for the elastic and inelastic channels, respectively. All widths are in the c.m. system.

E_p (MeV)	E_x (MeV)	J^π	Γ_T (keV)	Γ_e (keV)	l_0	s_0	$\gamma_{p_0 l_0 s_0}^2$ (keV)	Γ_i (keV)	l_1	$\gamma_{p_1 l_1}^{1/2^2}$ (keV)
3.88	10.91	$\frac{7}{2}^+$	90	90.0	2	$\frac{3}{2}$	0.110	0	$\cdots$	$\cdots$
3.90	10.93	$\frac{1}{2}^+$	90	36.0	0	$\frac{1}{2}$	0.013	54.0	0	0.071
3.99	11.01	$\frac{1}{2}^-$	20	15.4	1	$\frac{1}{2}$	0.008	4.6	1	0.014
4.13	11.14	$\cdots$	<10	<10	$\cdots$	$\cdots$	$\cdots$	$\cdots$	$\cdots$	$\cdots$
4.20	11.21	$\frac{1}{2}^+$	35	35	2	$\frac{3}{2}$	0.039	$\cdots$	$\cdots$	$\cdots$
4.575	11.56	$\cdots$	<10	<10	$\cdots$	$\cdots$	$\cdots$	$\cdots$	$\cdots$	$\cdots$
4.58	11.565	$\frac{5}{2}^-$	25	25	1, 3	$\frac{3}{2}, \frac{1}{2}$	0.005, 0.054	$\cdots$	$\cdots$	$\cdots$
4.63	11.61	$\frac{3}{2}^-(\frac{1}{2}^-)$	25	25	1	$\frac{3}{2}$	0.011	$\cdots$	$\cdots$	$\cdots$
4.74	11.71	$\cdots$	<10	<10	$\cdots$	$\cdots$	$\cdots$	$\cdots$	$\cdots$	$\cdots$
4.78	11.75	$\frac{5}{2}^+$	80	77.5	2	$\frac{3}{2}$	0.066	2.5	2	0.014
4.86	11.83	$\frac{5}{2}^-$	50	45.6	1	$\frac{3}{2}$	0.018	4.4	3	0.235
5.02	11.97	$\frac{5}{2}^-$	30	30	1, 3	$\frac{3}{2}, \frac{1}{2}$	0.007, 0.055	$\cdots$	$\cdots$	$\cdots$
5.18	12.12	$\frac{5}{2}^+$	160	160	2	$\frac{3}{2}$	0.116	$\cdots$	$\cdots$	$\cdots$
5.55	12.47	$\frac{5}{2}^-(\frac{3}{2}^-)$	60	58.3	1	$\frac{3}{2}$	0.020	1.7	3	0.067

The total inelastic cross section for an isolated resonance is given by

$$\sigma_i = \frac{\pi}{k^2} \frac{(2J+1)}{(2I_1+1)(2I_2+1)} \frac{\Gamma_e \Gamma_i}{(E_0+\Delta-E)^2+(\frac{1}{2}\Gamma)^2}. \quad (22)$$

Hence, if the total width and total inelastic cross sections are known, the elastic and inelastic widths (Γ_e and Γ_i, respectively,) can be determined.

RESULTS

A summary of the properties of the states in ^{15}O deduced from the present analysis is given in Table II. These parameters represent a best fit to the data and were used in the theoretical fits of Figs. 1–5. Alternate assignments of total spin, when they exist, are shown in parentheses.

Since resonance shapes for each partial-wave formation are quite distinct, it was possible to make reliable l-wave and parity assignments to the level analyzed. Resonance widths vary from ≤ 10 keV to a maximum of 160 keV and many of the levels are fairly broad and overlapping. Uncertainties associated with the resonant energies arise from experimental uncertainties in the absolute-energy measurement and from insensitivity of the fits to small variations in the resonant energies. Uncertainties associated with the widths are also due to the insensitivity of the fits.

In the elastic analyses, four resonances have the characteristic $l=1$ shape and four resonances have the characteristic $l=2$ shape. Resonances at 4.58 and 5.02

MeV could only be fit by assuming large contributions from two partial waves of $l=1, 3$. This is not unreasonable since the contribution from $l=3$ has a channel spin of $s=\frac{1}{2}$ and this channel spin is not allowed for the $l=1$ contribution (see Table I). If the level formation is channel-spin-dependent and favors $s=\frac{1}{2}$, then one would expect the $l=3$ contribution to be significant.

3.88, 3.90, and 3.99-MeV States

Two levels were observed in the elastic-scattering cross sections. The 3.88-MeV resonance is formed by $l=2$ as determined from the single-level shapes of Figs. 11 and 12. For this partial-wave formation, assignments of $J^\pi = \frac{1}{2}^+, \frac{3}{2}^+, \frac{5}{2}^+$, and $\frac{7}{2}^+$ are allowed. The assignments of $\frac{1}{2}^+$ and $\frac{3}{2}^+$ give theoretical cross sections that are much too small. The two most probable assignments are $\frac{5}{2}^+$ and $\frac{7}{2}^+$, but neither assignment gives a completely satisfactory fit. An admixture of $l=4$, which is also allowed for these assignments, does not improve the fit. This is not surprising since the penetrability of $l=4$ is down by a factor of 10.

The 3.99-MeV resonance shows a characteristic $l=1$ shape but nothing else can be said from a study of the elastic data. This resonance has a large inelastic width that has to be included in a detailed fit to the data.

Seven complete inelastic distributions (Fig. 5) were measured over the energy region of these resonances and the total inelastic cross section was obtained from a Legendre fit to these data. The elastic and inelastic widths were determined from the peak inelastic cross section with Eq. (4).

TABLE III. Legendre polynomial coefficients from least-squares fits to the inelastic angular distributions shown in Fig. 6.

E (MeV)	P_0	P_1	P_2	P_3	P_4
4.770	2.00	0.23	0.75	0.67	−0.63
4.801	2.16	0.10	0.62	1.46	−0.38
4.870	4.52	1.12	1.44	2.36	0.18
4.911	2.31	0.74	1.00	0.56	0.22
4.986	0.73	0.24	0.35	0.01	0.16

The angular distribution at 3.900 MeV is at the peak of the broad resonance and the one at 3.988 MeV is near the peak of the narrow resonance (see Figs. 3 and 4). Angular distributions over the broad resonance, taken at 3.868, 3.900, and 4.02 MeV, are far away from the interfering effects of the narrow resonance at 3.99 MeV and are nearly isotropic. The angular distributions at 3.966, 3.988, and 3.995 MeV taken in the vicinity of the narrow resonance indicate interference between levels of opposite parity. Initially it was assumed that the resonance observed at 3.88 MeV in the elastic cross section was the same resonance as that observed at 3.90 MeV in the inelastic cross section. The total widths of the two resonance peaks are about the same and the resonant energies differ by less than 20 keV. However, the inelastic angular distributions over the broad resonance at 3.9 MeV are inconsistent with the formation of an $l=2$ resonance as observed in the elastic cross section. Such a resonance predicts large P_2 and P_4 terms in a Legendre-polynomial expansion of the inelastic angular distribution, whereas an isotropic angular distribution is predicted only for a resonance formed through $l=0$. Since $l=0$ formation is definitely ruled out for the elastically observed resonance, the only acceptable explanation is the existence of two broad resonances, one with a large elastic width and the other with a large inelastic width.

Calculations were performed on the inelastic data with the assumption of a $\frac{1}{2}^+$, $\Gamma_T=90$-keV resonance at 3.9-MeV and a $\frac{1}{2}^-$, $\Gamma_T=20$-keV resonance at 3.987 MeV. The inelastic width of the 3.88-MeV level ($l=2$ formation) was taken to be zero. The total inelastic cross sections were determined to be 61 mb for the 3.9-MeV resonance and 43 mb for the 3.99-MeV resonance. Figures 3 and 4 show the fits to these data.

When the elastic widths for the $\frac{1}{2}^+$ and $\frac{1}{2}^-$ resonances, as determined from Eq. (4), were included in the elastic cross-section calculation and an assignment of $\frac{7}{2}^+$ was given to the 3.88-MeV resonance, a satisfactory fit (Figs. 1 and 2) was obtained. This assignment of $\frac{7}{2}^+$ to the elastic level at 3.88 MeV is consistent with the other $l=2$ assignments in this energy region. With this new interpretation of a third resonance, the assignment of $\frac{5}{2}^+$ for the 3.88-MeV level is eliminated.

4.2-MeV State

No inelastic cross section was observed, so the total width was assumed to be $\Gamma_T=\Gamma_e$. This resonance has the characteristic $l=2$ shape with probable assignments of $J^\pi=\frac{1}{2}^+$, $s=\frac{3}{2}$ or $J^\pi=\frac{3}{2}^+$, $s=\frac{1}{2}$. The $\frac{5}{2}^+$ or $\frac{7}{2}^+$ assignment is ruled out by the relatively small elastic cross section. An assignment of $J^\pi=\frac{3}{2}^+$, $s=\frac{3}{2}$ is not probable because, for this channel spin, the $l=0$ formation should dominate (see Table I). The assignment of $J^\pi=\frac{1}{2}^+$, $s=\frac{3}{2}$ represents the best fit and is also more consistent with the other $l=2$ assignments.

4.58- and 4.63-MeV States

The elastic cross sections revealed three closely spaced resonances with definite interference effects. There is no appreciable inelastic width for any of these resonances ($\Gamma_T=\Gamma_e$). The resonance at 4.58 MeV ($\Gamma_T=25$ keV) has a narrow resonance of less than 10 keV situated near its peak. This narrow resonance ($E_R\sim 4.575$ MeV) is small and does not destroy the characteristic shape of the 4.58-MeV resonance. The 4.58-MeV resonance does not show the characteristic shape of a single-partial-wave formation and can only be fit with an assignment of $J^\pi=\frac{5}{2}^-$, $l=1$, 3, $s=\frac{3}{2}$, $\frac{1}{2}$. No other assignments give the proper shape nor produce the observed interference with the 4.63-MeV resonance. The 4.63-MeV resonance has the characteristic shape of $l=1$ formation, but, as previously mentioned, it is distorted by interference from nearby levels. The best fit is obtained with $J^\pi=\frac{3}{2}^-$, $l=1$, $s=\frac{3}{2}$, $\Gamma=25$ keV. An alternate choice is $J^\pi=\frac{1}{2}^-$ but the fit is not as good at all angles.

4.78- and 4.86-MeV States

The resonances at 4.78 and 4.86 MeV overlap appreciably and definite interference effects are observed. A narrow level at 4.74 MeV was not analyzed. It has no detectable inelastic width and appears as a small bump in the elastic cross section. The 4.78-MeV resonance has the characteristic $l=2$ shape which is somewhat distorted by the 4.74-MeV resonance. The 4.86-MeV resonance has the characteristic $l=1$ shape. Tentative assignments of $J^\pi=\frac{5}{2}^+$, $s=\frac{1}{2}$, $\Gamma_T=80$ keV, $E_R=4.78$ MeV and $J^\pi=\frac{5}{2}^-$, $s=\frac{1}{2}$, $\Gamma_T=50$ keV, $E_R=4.86$ MeV were made from the elastic analysis. No other assignments gave satisfactory fits at all angles.

These two levels have significant partial widths for the inelastic channel (Figs. 3 and 4). Six inelastic angular distributions were taken over the energy region of these resonances and a least-squares Legendre polynomial fit was made to these data (Fig. 6). Estimated values of the total inelastic cross sections as determined from the angular-distribution measurements were 20 mb for the 4.78-MeV resonance and 50 mb for the 4.86-MeV level.

The Legendre-polynomial coefficients resulting from these least-squares fits are shown in Table III. Several important features were deduced from these coefficients.

(a) The two resonances are of opposite parity because odd polynomials appear in the angular distributions.

(b) Since the two resonances are of opposite parity, the even coefficients are a simple sum of the coefficients of the individual resonances; hence both resonances have significant P_2 and P_4 terms. The P_6 term is negligible.

(c) These resonances must have $J \geq \frac{5}{2}$ because resonances of small J value cannot have P_4 contributions.

(d) These resonances probably do not have $J \geq \frac{7}{2}$ because such assignments would result in P_6 contributions of the same order of magnitude as the P_0, P_2, and P_4 terms.

From a study of these coefficients, we conclude that the resonances are of opposite parity and most probably have $J = \frac{5}{2}$. Assignments from the elastic analysis are $\frac{5}{2}^+$ for the 4.78-MeV resonance and $\frac{5}{2}^-$ for the 4.86-MeV resonance.

Exact fits to these higher-order angular distributions are complicated by the large number of interference terms present and by the many possible channel-spin configurations. Furthermore, the interference terms are quite sensitive to the potential phase shifts of elastic and inelastic scattering; since these are not known exactly, they must at best be treated as adjustable parameters. More complete inelastic data are needed for such an analysis.

5.02-MeV State

This resonance is peaked at all angles and does not exhibit the characteristic shape of a single-partial-wave formation. An $l=4$ formation is peaked at all angles, but the magnitude and detailed shape are not consistent with this assignment. A combination of $l=1$ and $l=3$ produce the desired effects and result in an assignment of $J^\pi = \frac{5}{2}^-$. The resonance at 4.58 MeV has a similar shape and was also fit with this assignment. Differences in shapes of these two resonances are attributed to interference from nearby levels and to variations in the nonresonant phase shifts at the two energies. An assignment of $J^\pi = \frac{5}{2}^-$, $l=1$, 3, $s=\frac{1}{2}$, $\frac{3}{2}$, and $\Gamma_T = 30$ keV gave the best fit.

5.18-MeV State

This broad resonance ($\Gamma_T = 160$ keV) has the characteristic $l=2$ shape. The inelastic cross section is not sufficiently large to be extracted from an apparent nonresonant background (See Figs. 3 and 4). A best fit is obtained with an assignment of $J^\pi = \frac{5}{2}^+$, $l=2$, $s=\frac{3}{2}$ which is consistent with the other $l=2$ assignments. No other $l=2$ assignments gave an acceptable fit.

5.55-MeV State

Cross sections were detected for the $^{14}N(p, p_1)^{14}N^*$, $^{14}N(p, p_2)^{14}N^*$, and $^{14}N(p, \alpha)^{11}C$ reactions, but their widths were much smaller than the corresponding elastic width. An inelastic angular distribution over this resonance (Fig. 6) is not symmetric about 90° c.m., indicating interference with the nonresonant background or with levels of opposite parity. Incomplete reaction data and background interference prevented the extraction of reliable reaction widths. This resonance exhibited the characteristic $l=1$ shape and was fit with an assignment of $J^\pi = \frac{5}{2}^-$, $l=1$, $s=\frac{3}{2}$, and $\Gamma_T = 60$ keV. Another possible assignment is $\frac{3}{2}^-$, but the fit is not as good at the backward angles.

DISCUSSION

We will not try to interpret the properties of the observed levels in terms of nuclear models since the situation at these excitation energies is quite complicated. It is interesting to note, however, that Shukla and Brown[26] have recently reported an extensive theoretical interpretation of the properties of excited states of the mass-15 nuclei. These authors construct the $\frac{1}{2}^-$ and $\frac{3}{2}^-$ states by mixing single-hole spherical and two-particle–three-hole deformed configurations. The even-parity states are constructed by mixing one-particle–two-hole and three-particle–four-hole deformed states. This interpretation of states in ^{15}O extends up to excitation energies of about 10 MeV, which is just below the region we have studied. In fact, these authors predict a $\frac{1}{2}^-$ state which may be the state observed at 11.01-MeV excitation.

Our hope is that modern theoretical techniques will be equal to the complexity of the energy region which we have studied and that the properties of states identified in this work will be valuable in future theoretical interpretations of the ^{15}O nucleus.

[26] A. P. Shukla and G. E. Brown, Nucl. Phys. **A112**, 296 (1968).